Entropy-driven docosahedral short-range order in simple liquids and glasses

Kengo Nishio,* Anh Khoa Augustin Lu, and Takehide Miyazaki
National Institute of Advanced Industrial Science and Technology (AIST), Central 2, Umezono 1-1-1, Tsukuba, Ibaraki 305-8568, Japan

(Received 2 May 2018; revised manuscript received 16 October 2018; published 13 February 2019)

The *energetically favored* icosahedral structure has been seen as the central figure for describing the local structure of simple liquids and glasses. Although regular icosahedral structures are rarely found, it is accepted that distorted icosahedral structures occur in simple liquids and glasses. However, which local structure dominates and why it is more frequent than the others remain unanswered questions. In this study, by using a recently developed structure descriptor, we show that docosahedral structures are the most favored not only in models of simple liquids and glasses but also in an experimental colloid glass. We also show that the the predominance of docosahedral structures is *entropy-driven*. Our findings represent a significant milestone towards comprehending mysterious phenomena such as supercooling, glass transition, and crystallization, where local structures play a key role.

DOI: 10.1103/PhysRevE.99.022121

I. INTRODUCTION

Liquid is one of the three major states of matter. Since its atomic structure is believed to be related to mysterious phenomena such as supercooling, glass transition, and crystallization, enormous effort has been devoted to its understanding. Simple liquids, which consist of identical spherical atoms, are one of the simplest classes of disordered systems. Even for this simple case, the atomic structure remains poorly understood. A tendency to favor a particular type of local structure (a structure composed of a central atom and its neighbors) is called short-range order. It is well known that, at a shorter-range scale, four neighboring atoms in simple liquids tend to form a regular tetrahedral structure [1–3]. However, it remains mysterious how the tetrahedral order develops into the short-range order.

To explain the supercooling phenomenon [4], Frank proposed that simple liquids contain many icosahedral local structures [5]. This hypothesis is based on the energetic analysis of arrangements of 13 atoms interacting via a Lennard-Jones (LJ) potential: an icosahedral cluster has a lower energy than a face-centered-cubic (fcc) and a hexagonal close-packed (hcp) cluster. Frank's argument has been a good working hypothesis motivating numerous studies of the structure of disordered systems [2,6–22]. A few papers were against this hypothesis, for nearly regular icosahedral structures were rarely found in the LJ liquid or the modified LJ liquid [19–22]. On the other hand, many others advocated it by assuming that icosahedral structures include not only regular icosahedral structures but also distorted (or defective) icosahedral structures [2,6–15]. However, the term "distorted icosahedron" is ambiguous. Some authors meant a local structure with a value of the W_6 order parameter below a certain threshold [6,7,11], some meant a thermally vibrated regular or twisted icosahedral structure [10,13], and some meant a local structure with a Voronoi index $\langle 0, 2, 8, 1\rangle$, $\langle 0, 2, 8, 2\rangle$, or $\langle 0, 1, 10, 2\rangle$ [8]. Thus, a clear picture of the local structure is still missing.

In contrast to Frank's energetic approach, Bernal proposed the dense random packing of hard spheres as a structure model of simple liquids [1,3,23–25]. This model ignores energetic effects but captures entropic ones. Despite the fact that the density assigned to a local structure is maximized for a regular icosahedral structure [26], it is well known that icosahedral structures are rarely found in the hard-sphere system [3,23–25]. We point out that there is an overlooked paradox between the currently accepted picture of the hard-sphere system and that of the LJ liquid. Purely entropic effects determine the local structure of the hard-sphere system, while it is generally believed that the energetic effects dominate that of the LJ liquid. Nevertheless, the hard-sphere packing reproduces the overall features of the radial distribution function of liquid Ar [1,25], which is well reproduced by the LJ potential.

The questions of which local structure dominates in simple liquids and why it is more frequent than the others still remain unanswered. The lack of the fundamental understanding of the local structure stems from a profound but overlooked problem: although a liquid consists of an unlimited variety of local structures, there was no reliable method for classifying them. A popular approach to studying the atomic arrangement is to represent it as a tiling of Voronoi polyhedra [7,8,12,18,23–25,27–31] [Fig. 1(a)]. Each polyhedron contains one atom, and the shape of the polyhedron corresponds to the local structure [Fig. 1(b)]. The short-range order of disordered structures has been investigated by classifying their Voronoi polyhedra according to the Voronoi indices. Although the Voronoi index specifies how many i-gons ($i = 3$, 4, 5, ...) are contained in a polyhedron, it does not specify how these polygons are arranged. As a result, different polyhedra may have the same index [7,27,29,32]. This degeneracy prevents proper classification of the local structures. The Voronoi index analysis of disordered structures thus potentially leads to a misunderstanding of their short-range order.

*k-nishio@aist.go.jp

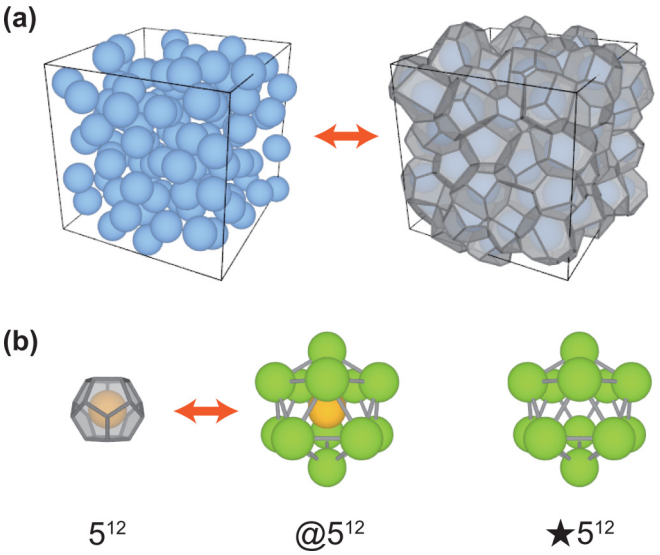

FIG. 1. Method for describing the atomic arrangements. (a) The arrangement of atoms can be represented as a tiling of Voronoi polyhedra. (b) Relation between a Voronoi polyhedron and its corresponding local structure. By using the p_3 codeword [27–29], the Voronoi polyhedron associated with the central atom (orange) is represented by 5^{12} (dodecahedron). The polyhedron formed by the atoms (green) surrounding the central one is the dual of the 5^{12}-polyhedron and is represented by ★5^{12} (icosahedron). The local structure composed of the central (orange) and its neighbors (green) is represented by @5^{12} (icosahedral structure).

To paraphrase Galileo's *Il Saggiatore* [33], mathematics for classifying the local structures is necessary to comprehend disordered structures. We therefore developed a method for giving a unique codeword (which we call p_3) to any polyhedron in terms of how the building-block polygons are arranged to form that polyhedron [27–29]. In the present study, we apply this method to elucidate the short-range order in simple liquids and glasses: the LJ liquid, from which the Frank's hypothesis originates [5], the LJ glass, the dense random packing of hard spheres, and even an experimental colloid glass [34].

II. METHOD

A. Brief explanation of p_3 codeword

A polyhedron is constructed by gluing polygons side to side. By using a recently developed mathematical method called the p_3-code [27–29], any polyhedron can be represented by a unique codeword p_3, in which the information of how the building-block polygons are arranged is stored. In general, a p_3 codeword consists of a polygon-sequence codeword (ps_2) and a side-pairing codeword (sp) and is expressed as $p_3 = ps_2; sp$, where ";" is a separator. However, all the p_3 codewords of the Voronoi polyhedra found in this work do not contain sp, namely, $p_3 = ps_2$. The ps_2 codeword is expressed as $ps_2 = p_2(1)p_2(2)p_2(3)\cdots p_2(F)$. Here $p_2(i)$ is the number of sides of the ith polygon. F is the number of polygons of the polyhedron. Each $p_2(i)$ indicates the ith building-block polygon, and the sequence of the $p_2(i)$'s designates how to assemble the building-block polygons into a polyhedron. By using a decoding algorithm [27–29], the original polyhedron (combinatorial structure) can be reconstructed from its p_3 codeword.

A polyhedron represented by p_3 is henceforth called a p_3-polyhedron. Figure 1(b) briefly illustrates how a local structure is represented by using p_3. When the Voronoi polyhedron associated with an atom is a p_3-polyhedron, its neighboring atoms are placed at the vertices of a ★p_3-polyhedron, where ★p_3 denotes the dual of a p_3-polyhedron. The arrangement of the central atom and its neighbors is represented by @p_3. Thus, "@" is the symbol that links a Voronoi polyhedron to its corresponding local structure.

Note that there are several methods for classifying polyhedra. For example, polyhedra can be classified according to the t-indices [35], which were developed for classifying the hydrogen network of ice clusters. However, the t-index is significantly lengthy. Polyhedra can also be classified according to the Weinberg codewords [36], which were developed for classifying planer-triply connected graphs. The Weinberg codeword is less redundant than the t-index. However, it is still lengthy. For example, the Weinberg codeword of a dodecahedron is "1 2 3 4 5 1 5 6 7 8 1 8 9 10 2 10 11 12 3 12 13 14 4 14 15 6 15 16 17 7 17 18 9 18 19 11 19 20 13 20 16 20 19 18 17 16 15 14 13 12 11 10 9 8 7 6 5 4 3 2 1." The same polyhedron is briefly encoded as 5^{12} by using the p_3 code [27–29]. We emphasize that the p_3-code is designed to describe local structures [Fig. 1(b)]. In contrast, both the t-index and the Weinberg codeword are not designed for describing local structures. Therefore, they can denote a Voronoi polyhedron, but they are unable to designate the corresponding local structure.

B. Lennard-Jones systems

The LJ liquid is a representative model of simple liquids such as rare-gas liquids and metallic liquids. The LJ potential [37,38] is expressed as

$$\phi_{\mathrm{LJ}}(r) = 4\epsilon\left[\left(\frac{\sigma}{r}\right)^{12} - \left(\frac{\sigma}{r}\right)^{6}\right]. \tag{1}$$

Here r is the distance between the two atoms, ϵ is the potential well depth, and σ is the distance at which the potential becomes zero. The triple point temperature and pressure of the LJ system are $T_{\mathrm{tp}} = 0.694\epsilon$ and $P_{\mathrm{tp}} = 0.0203\epsilon/\sigma^3$, respectively [39]. As an example, we use the parameter values for Ar [37], namely, $\epsilon/k_{\mathrm{B}} = 120$ [K] and $\sigma = 3.4$ [Å], where k_{B} is the Boltzmann constant. In this case, $T_{\mathrm{tp}} = 83.3$ [K] and $P_{\mathrm{tp}} = 0.86$ [MPa]. We cut off the interaction at a distance of 4σ. To remove the discontinuity of the potential, we use a cut-and-shifted potential expressed as

$$\phi_{\text{cs-LJ}}(r) = \begin{cases} \phi_{\mathrm{LJ}}(r) - \phi_{\mathrm{LJ}}(4\sigma) & (0 < r \leqslant 4\sigma) \\ 0 & (4\sigma < r) \end{cases}. \tag{2}$$

We study liquids composed of 6912 atoms at different temperatures and pressures: $(T, P) = (0.80T_{\mathrm{tp}}, P_{\mathrm{tp}})$, $(T_{\mathrm{tp}}, P_{\mathrm{tp}})$, $(0.90T_{\mathrm{tp}}, 49.20P_{\mathrm{tp}})$, and $(1.12T_{\mathrm{tp}}, 49.20P_{\mathrm{tp}})$. Note that the melting point is $1.12T_{\mathrm{tp}}$ at a pressure of $49.20P_{\mathrm{tp}}$ [39]. We use a self-developed program to perform isothermal-isobaric molecular dynamics simulations. We solve Hamilton's equations derived from a Poincaré transform of the Nosé-Andersen

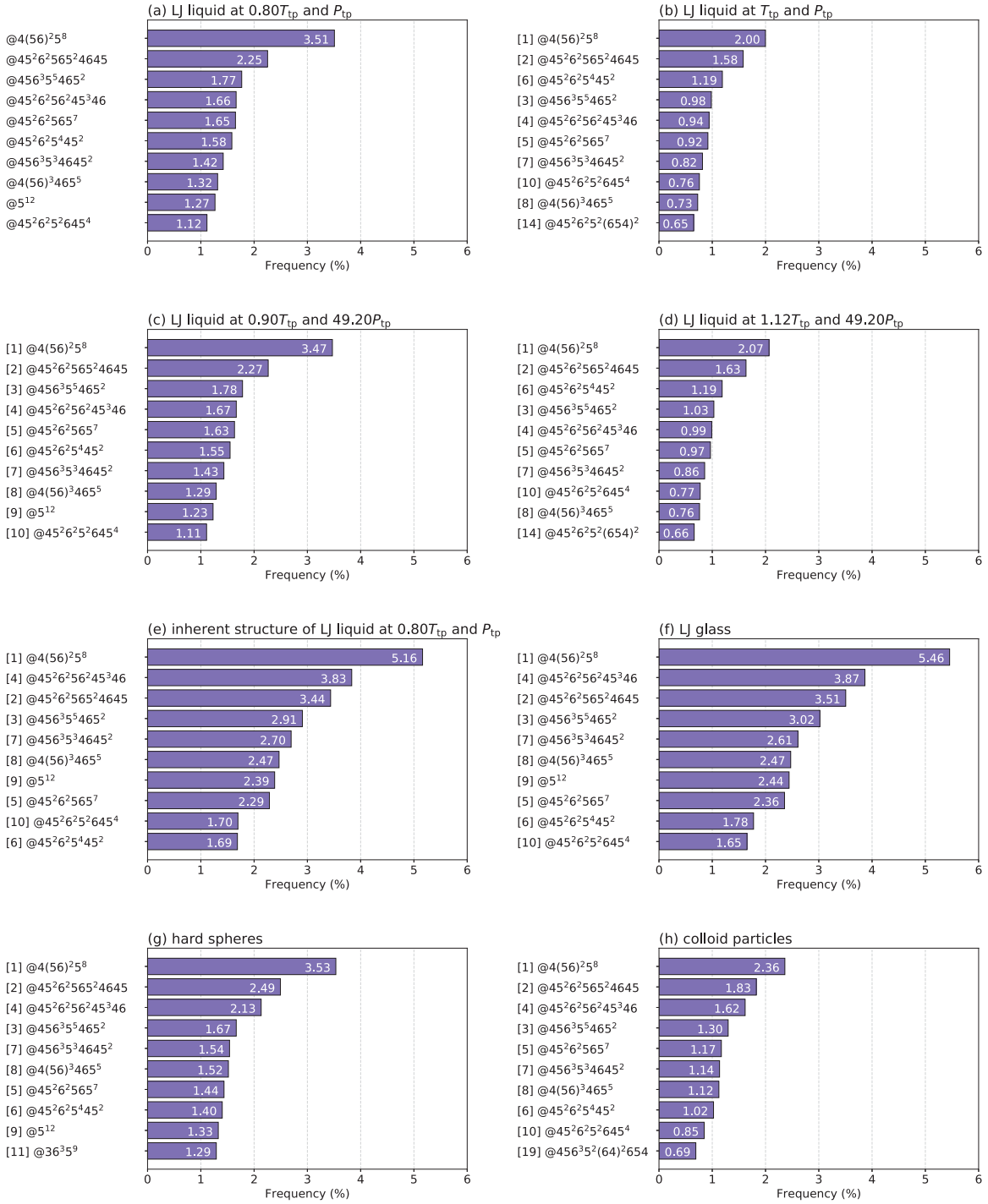

FIG. 2. Distribution of most frequent local structures for (a) the LJ liquid at $0.80T_{tp}$ and P_{tp}, (b) the LJ liquid at T_{tp} and P_{tp}, (c) the LJ liquid at $0.90T_{tp}$ and $49.20P_{tp}$, (d) the LJ liquid at $1.12T_{tp}$ and $49.20P_{tp}$, (e) the inherent structure of the LJ liquid at $0.80T_{tp}$ and P_{tp}, (f) the LJ glass, (g) the dense random packing of hard spheres, and (h) the experimental dense random packing of colloid particles [34]. Each number in brackets on the left of the @ symbol indicates the rank in the LJ liquid at $0.80T_{tp}$ and P_{tp}.

Hamiltonian [40–44] using the integrator described in the Appendix. After equilibrating each system for more than 20 ps, we perform a 100-ps simulation. We analyze the atomic configuration every 0.01 ps. Thus, a total of 10 000 atomic configurations are analyzed. We also construct inherent structures of the LJ liquid at $0.80T_{tp}$ and P_{tp} by optimizing the instantaneous atomic configurations and cell volume every 10 ps, and analyze a total of 10 inherent structures. In addition, we study a total of 10 LJ glasses. To generate a glass, we cool a liquid from T_{tp} to $0.004T_{tp}$ at a pressure of P_{tp} at a cooling rate of 10^{13} K/s, and then optimize the atomic configurations and cell volume.

For reference, we also study a fcc crystal composed of 864 atoms, hcp crystal composed of 448 atoms, and bcc crystal

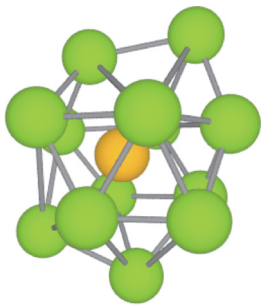

FIG. 3. Docosahedral structure ($@4(56)^2 5^8$) found in the LJ liquid at a temperature of $0.80T_{tp}$ and pressure of P_{tp}. It consists of a central atom (orange) and its 13 neighbors (green) placed at the vertices of a docosahedron ($\bigstar 4(56)^2 5^8$-polyhedron).

composed of 686 atoms at a temperature of $0.80T_{tp}$ and pressure of P_{tp}. We use isothermal-isobaric molecular dynamics simulations for the fcc and bcc crystals. However, since the hcp crystal is not a cubic crystal system, the Nosé-Andersen method cannot be used for it. We therefore perform isothermal molecular dynamics simulations by solving Hamiltonian's equations derived from a Poincaré transform of the Nosé Hamiltonian [41,42]. In this case, a rectangular simulation cell is used. The values of the cell parameters are fixed so that the density of the hcp crystal equals that of the fcc crystal. For each crystal, we perform five independent 100-ps simulations, and a total of 50 000 atomic configurations are analyzed.

C. Dense random packing of hard spheres

We generate a total of 10 dense random packings of 6912 hard spheres using DynamO [45], an event-driven molecular dynamics program. We first generate hard-sphere fluids with packing densities of 0.1, 0.2, 0.3, 0.4, and 0.5. For each packing density, two structures are generated: one is obtained after 10^6 collisions, while the other is after 2×10^6 collisions. The 10 structures are compressed to obtain dense random packings with a packing density of 0.637, which is close to a maximum random packing density [1,25].

TABLE I. Frequency of occurrence of most frequent local structures found in the LJ liquid at a temperature of $0.8T_{tp}$ and pressure of P_{tp}. A rank vector (l, f, h, b) is assigned to each structure. Here l, f, h, and b are the ranks in the liquid, fcc crystal, hcp crystal, and bcc crystal, respectively. For example, the rank vector(1, 25, 37, 57) for $@4(56)^2 5^8$ indicates that this structure ranks first in the liquid, 25th in the fcc crystal, 37th in the hcp crystal, and 57th in the bcc crystal. A minus sign means that the considered structure is not found. For example, the minus sign in the rank vector(5, −, −, 206) of $@45^2 6^2 565^7$ indicates that this structure is not found in the fcc and hcp crystals.

Local structure	Frequency (%)	Rank	vector	$(l, f,$	$h, b)$
$@4(56)^2 5^8$	3.51	(1,	25,	37,	57)
$@45^2 6^2 565^2 4645$	2.25	(2,	5,	1,	16)
$@456^3 5^5 465^2$	1.77	(3,	1405,	34,	29)
$@45^2 6^2 56^2 45^3 46$	1.66	(4,	2,	7,	18)
$@45^2 6^2 565^7$	1.65	(5,	−,	−,	206)
$@45^2 6^2 5^4 45^2$	1.58	(6,	30,	44,	107)
$@456^3 5^3 4645^2$	1.42	(7,	8,	19,	11)
$@4(56)^3 465^5$	1.32	(8,	12,	28,	47)
$@5^{12}$	1.27	(9,	101,	99,	449)
$@45^2 6^2 5^2 645^4$	1.12	(10,	1006,	31,	62)

TABLE II. Frequency of occurrence of most frequent local structures found in the fcc crystal of the LJ system at a temperature of $0.8T_{tp}$ and pressure of P_{tp}.

Local structure	Frequency (%)	Rank	vector	$(l, f,$	$h, b)$
$@45^2 6^5 4645^2 46$	9.52	(88,	1,	32,	23)
$@45^2 6^2 56^2 45^3 46$	6.99	(4,	2,	7,	18)
$@4(56)^3 465(64)^2$	5.86	(22,	3,	3,	7)
$@456^3 5645^2 (46)^2$	5.62	(26,	4,	30,	14)
$@45^2 6^2 565^2 4645$	4.88	(2,	5,	1,	16)
$@45^3 6^5 46454$	4.55	(143,	6,	26,	12)
$@45^2 6^3 5645464$	4.01	(23,	7,	15,	9)
$@456^3 5^3 4645^2$	3.28	(7,	8,	19,	11)
$@45^3 6^5 45^2 45$	3.16	(270,	9,	2825,	60)
$@45^2 6^2 56^2 45645^2$	3.05	(119,	10,	−,	103)

D. Experimental colloid glass

Kurita and Weeks experimentally generated a dense random packing of colloid particles and determined the three-dimensional positions of the particle centers by using confocal microscopy [34]. They provided the coordination data set for the colloid glass with a size of $492 \times 514 \times 28$ [μm^3] containing 453 136 particles. To remove the surface effects, we analyze the 183 030 particles far away from the surfaces.

III. RESULTS AND DISCUSSION

The distributions of most frequent local structures found in the LJ liquids at $(0.80T_{tp}, P_{tp})$, (T_{tp}, P_{tp}), $(0.90T_{tp}, 49.20P_{tp})$, and $(1.12T_{tp}, 49.20P_{tp})$ are shown in Figs. 2(a), 2(b), 2(c), and 2(d), respectively. In all the cases, the most frequent type of local structure is the 14-atom structure represented by $@4(56)^2 5^8$ (Fig. 3). The distribution for the inherent structure of the LJ liquid at $0.80T_{tp}$ and P_{tp}, where thermal motion is frozen, is also shown in Fig. 2(e). As with the parent liquid, docosahedral structures are dominant in the inherent structure.

TABLE III. Frequency of occurrence of most frequent local structures found in the hcp crystal of the LJ system at a temperature of $0.8T_{tp}$ and pressure of P_{tp}.

Local structure	Frequency (%)	Rank	vector	$(l, f,$	$h, b)$
$@45^2 6^2 565^2 4645$	4.62	(2,	5,	1,	16)
$@4(56)^3 46^2 4654$	4.16	(30,	937,	2,	8)
$@4(56)^3 465(64)^2$	3.60	(22,	3,	3,	7)
$@456^3 5^2 (64)^2 654$	3.59	(19,	17,	4,	2)
$@45^2 6^2 565^3 (64)^2$	3.56	(17,	1130,	5,	36)
$@45^2 6^3 5645^2 456$	3.25	(24,	−,	6,	22)
$@45^2 6^2 56^2 45^3 46$	3.13	(4,	2,	7,	18)
$@4(56)^2 (6^2 4)^2 (64)^2$	2.70	(138,	15,	8,	3)
$@45^2 6^2 5^2 (654)^2$	2.52	(14,	1561,	9,	13)
$@456^3 (564)^2 6564$	2.36	(37,	13,	10,	10)

TABLE IV. Frequency of occurrence of most frequent local structures found in the bcc crystal of the LJ system at a temperature of $0.8T_{tp}$ and pressure of P_{tp}.

Local structure	Frequency (%)	Rank	vector	$(l, f,$	$h, b)$
$@46^4(46)^44$	50.06	(185,	24,	21,	1)
$@456^35^2(64)^2654$	9.95	(19,	17,	4,	2)
$@4(56)^2(6^24)^2(64)^2$	8.17	(138,	15,	8,	3)
$@456^3465(46)^24$	8.00	(44,	11,	11,	4)
$@367^2(46)^245(46)^2$	2.16	(205,	66,	66,	5)
$@357^26^2(46)^44$	2.16	(481,	65,	67,	6)
$@4(56)^3465(64)^2$	1.95	(22,	3,	3,	7)
$@4(56)^346^24654$	1.54	(30,	937,	2,	8)
$@45^26^35645464$	1.19	(23,	7,	15,	9)
$@456^3(564)^26564$	1.14	(37,	13,	10,	10)

Essentially the same result is also obtained for the LJ glass [Fig. 2(f)]. We call an $@4(56)^25^8$ structure a docosahedral structure because it consists of a central atom and its 13 neighbors placed at the vertices of a docosahedron [★$4(56)^25^8$-polyhedron]. The predominance of docosahedral structures distinguishes the liquid from crystals. In fact, the rank vector of $@4(56)^25^8$ is (1, 25, 37, 57), meaning that $@4(56)^25^8$ ranks 1st in the liquid, 25th in an fcc crystal, 37th in an hcp crystal, and 57th in a bcc crystal (Table I). Note that the most frequent type of local structures in the fcc crystal, the hcp crystal, and the body-centered-cubic (bcc) crystal are $@45^26^54645^246$ (Table II), $@45^26^2565^24645$ (Table III), and $@46^4(46)^44$, respectively (Table IV).

The 10 most frequent local structures in the LJ liquid at a temperature of $0.80T_{tp}$ and P_{tp} are derivatives of the (parent) docosahedral structure (Fig. 4). In fact, the

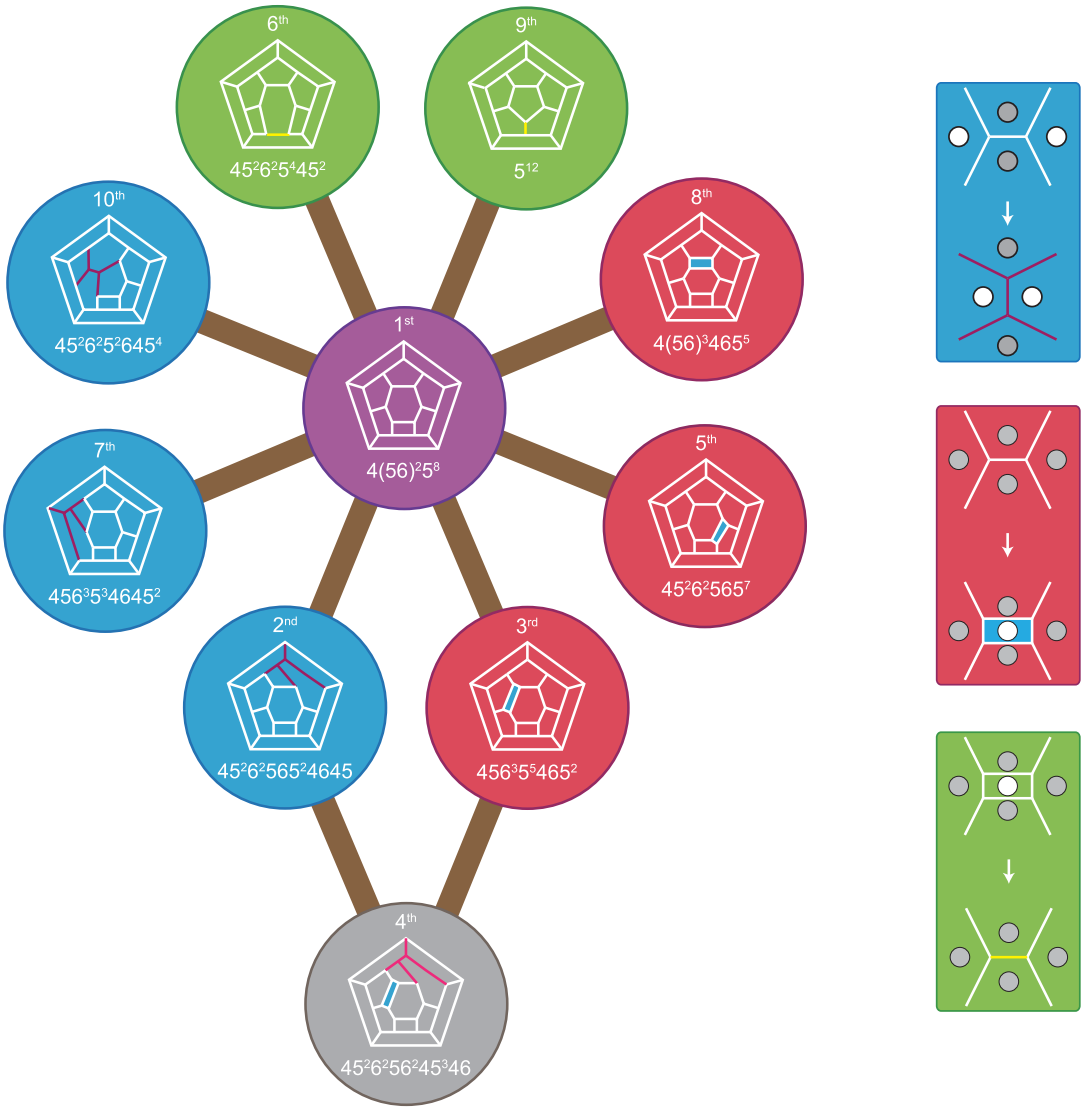

FIG. 4. Relation between the docosahedral structure ($@4(56)^25^8$) and its derivatives at a temperature of $0.80T_{tp}$ and pressure of P_{tp}. The local structures are represented by graphs of the corresponding Voronoi polyhedra. The blue, red, and green insets on the right schematically illustrate the effects of local atomic rearrangement, addition of an atom, and removal of an atom, respectively. The structures corresponding to the blue graphs can be obtained by locally rearranging atoms of the docosahedral structure. The red structures can be obtained by adding an atom to the docosahedral structure. The green structures can be obtained by removing an atom from the docosahedral structure. The gray structure can be obtained either by adding an atom to the second-ranked structure or by locally rearranging the third-ranked structure.

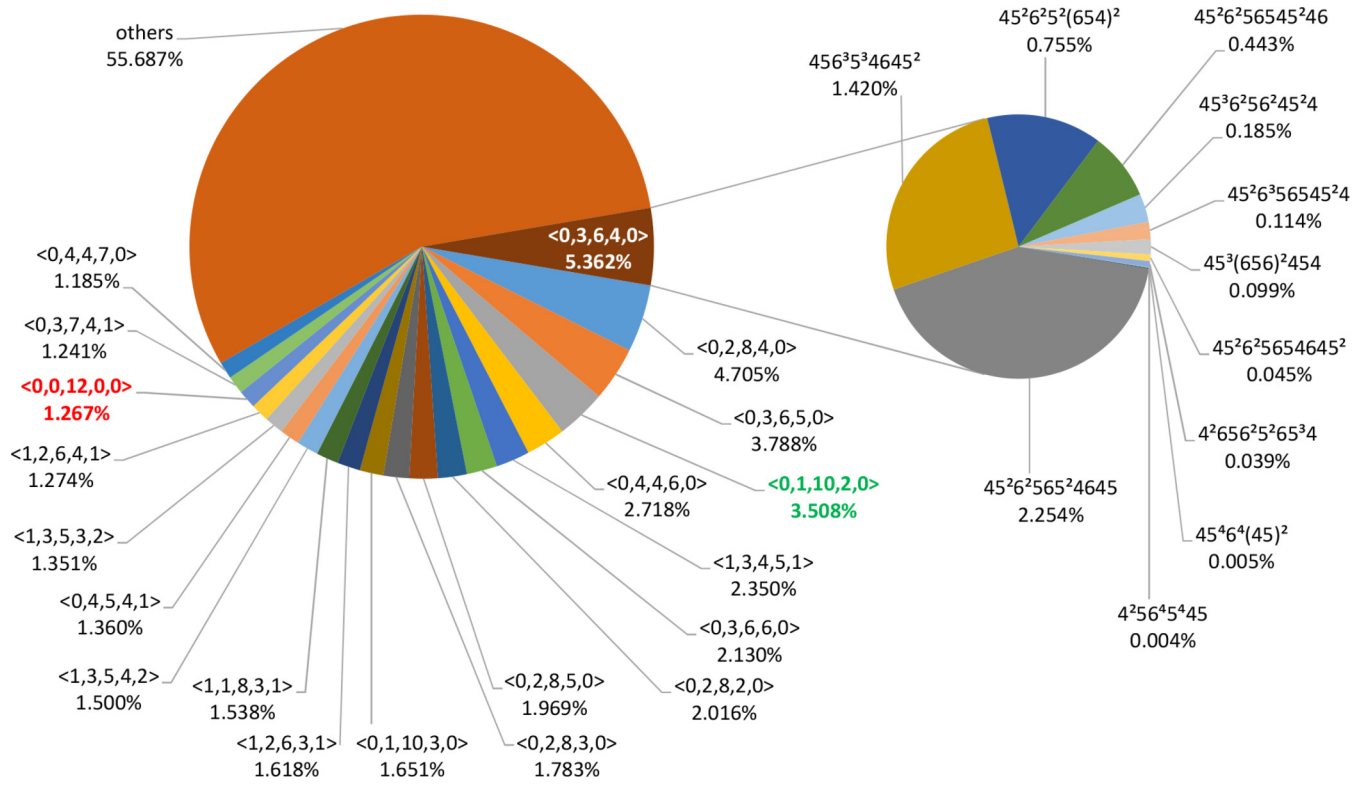

FIG. 5. Distribution of most frequent Voronoi indices for the LJ liquid at a temperature of $0.80T_{\rm tp}$ and pressure of $P_{\rm tp}$. For the secondary pie chart on the right, the labels are p_3 codewords. Note that $\langle 0, 1, 10, 2\rangle$ corresponding to the docosahedron ranks fourth, while $\langle 0, 0, 12, 0\rangle$ corresponding to the icosahedron ranks 18th.

$@45^26^256^24645$ (ranked second), $@456^35^34645^2$ (seventh), and $@45^26^25^2645^4$ (10th) structures can be obtained from the docosahedral structure by locally rearranging the atoms. The $@456^35^5465^2$ (third), $@45^26^256^7$ (fifth), and $@4(56)^3465^5$ (eighth) structures can be obtained by adding a 15th atom to the docosahedral structure, while the $@45^26^25^445^2$ (sixth) and $@5^{12}$ (ninth) structures can be obtained by removing an atom. The $@45^26^256^245^346$ (fourth) structure can be obtained either by adding a 15th atom to the second-ranked structure or by locally rearranging atoms of the third-ranked one. Note that the icosahedral structure ($@5^{12}$) is merely one of the derivatives, ranking ninth.

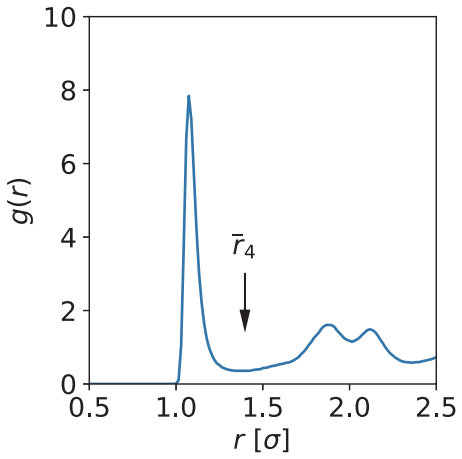

FIG. 6. Radial distribution function (g(r)) of the LJ glass. The arrow indicates the position corresponding to the average distance ($\bar{r}_4$) of the central atom of the docosahedral structure to its neighbor corresponding to the square face of the Voronoi polyhedron.

The previous Voronoi index analyses overlooked the importance of docosahedral structures [7,31] since the most frequent Voronoi index is $\langle 0, 3, 6, 4\rangle$. However, the high frequency of occurrence of $\langle 0, 3, 6, 4\rangle$ arises merely because the Voronoi index fails to distinguish different types of polyhedra. In fact, our p_3 analysis shows that as many as 11 different polyhedra have the same index $\langle 0, 3, 6, 4\rangle$ (Fig. 5). As a result, we uncover the importance of docosahedral structures. The docosahedral structure, which has a Voronoi index of $\langle 0, 1, 10, 2\rangle$, has been regarded as a distorted icosahedral structure. However, this is unreasonable for the following two reasons. First, this is a category error. Given that the docosahedron is a polyhedron with 22 faces, while the icosahedron has 20 faces, a docosahedron will not be any type of icosahedron. Second, the atoms in simple liquids tend to form the docosahedral structure, and icosahedral structures are formed only when atoms fail to do it. Thus, not the icosahedral but the docosahedral structure is the central figure for describing the local structure.

To identify the origin of the docosahedral short-range order of the LJ liquid, we first define the energy e_i of the atom i as

$$e_i = \frac{1}{2}\sum_j \phi_{\text{cs-LJ}}(r_{ij}). \tag{3}$$

Here r_{ij} is the distance between the atoms i and j. The average of e_is of the central atoms and their neighbors of the docosahedral structures in the inherent structure of the LJ liquid ($\bar{e}_{\rm doc} = -7.65\epsilon$) is higher than that of the icosahedral structures ($\bar{e}_{\rm ico} = -7.68\epsilon$). In other words, docosahedral structures are energetically less favored than icosahedral structures. In addition, as with the LJ liquid, docosahedral order dominates in the dense random packing of hard spheres [Fig. 2(g)]. These results provide firm evidence that the docosahedral order of the LJ systems is entropy-driven, disproving the generally accepted picture that the energetic effects dominate the local structure of simple liquids.

The entropy maximization of a hard-sphere system can be achieved by optimizing local sphere packing [46]. Although the density assigned to a local structure is maximized for a regular icosahedral structure [26], there are gaps between the atoms. When some gaps are narrowed by rearranging the atoms, the other gaps are inevitably enlarged. As a result, an additional 14th atom fits in one of the enlarged gaps of a 13-atom local structure such as $@5^{12}$ and $@45^26^25^445^2$ to form a docosahedral structure. This is the reason why docosahedral structures are favored in simple liquids, but regular icosahedral structures are not.

To identify which atom is the 14th atom, we calculate the average distance $\bar{r}_i$ of the central atom of the docosahedral structure to its neighbor corresponding to the i-gonal face of the Voronoi polyhedron. Note that the central atom of a docosahedral structure has one neighbor corresponding to the square, 10 neighbors corresponding to the pentagons, and two neighbors corresponding to the hexagons. $\bar{r}_4$, $\bar{r}_5$, and $\bar{r}_6$ of the LJ glass are 1.40, 1.12, and 1.07σ, respectively. Thus, the atom corresponding to the square is found to be the additional one. Essentially the same results are obtained for the inherent structure of the LJ liquid. As well known [7] and as illustrated in Fig. 6, the first and second peaks of the radial distribution function of the LJ glass is not separated. The $\bar{r}_4$ lies between the position of the first peak and that of the second one. Thus, the nonseparated peaks are a sign of the docosahedral structure.

Finally, we demonstrate the presence of docosahedral order in an experimental sample: a dense random packing of colloid particles [34]. Figure 2(g) illustrates that docosahedral order is also dominant in the experimental colloid glass despite the fact that the colloid particles has a polydispersity of 5% in their diameters.

IV. CONCLUSION

By combining the recently developed p_3 codeword and molecular dynamics simulations, we have demonstrated that docosahedral order is dominant in the LJ liquid and glass. The docosahedral order is entropy-driven because docosahedral structures are energetically less favored than icosahedral structures and also dominant in the dense random packing of hard spheres. Thus, we disprove the misconception that the energetic effects dominate the local structure of simple liquids. As a result, the paradox in the generally accepted pictures of the hard-sphere system and the LJ liquid has been resolved. We have also shown that docosahedral order is dominant in the experimental colloid glass, strengthening the reliability of our theoretical prediction. Our observation that docosahedral order is dominant independently of the details in atomic interactions and thermodynamic conditions represents the robustness and importance of docosahedral order in disordered systems composed of spherical particles. The role of icosahedral structures in fundamental phenomena such as supercooling, glass transition, and crystallization in simple liquids has been extensively studied from the 1950s to the present [2,5–7,10–14,18,30,47]. However, our findings suggest that further attention should be paid to the most frequent docosahedral structures to comprehend those phenomena.

ACKNOWLEDGMENT

K.N. wishes to thank A. Hirata for fruitful discussions.

APPENDIX: INTEGRATOR FOR ISOTHERMAL-ISOBARIC MOLECULAR-DYNAMICS SIMULATIONS

A Poincaré transform [41] of the Nosé-Andersen Hamiltonian $H_{\rm NA}$ [43,44] is expressed as

$$\begin{aligned} H &= s[H_{\rm NA} - H_0] \\ &= s\left[\sum_{i=1}^{N} \frac{\hat{\boldsymbol{p}}_i^2}{2m_i V^{\frac{2}{3}} s^2} + U(V^{\frac{1}{3}}\hat{\boldsymbol{q}}) + \frac{\pi^2}{2Q}\right. \\ &\quad \left. + \left[3Nk_{\rm B}T\ln(s) + \frac{P_V^2}{2W} + PV - H_0\right]\right]. \end{aligned} \tag{A1}$$

Here $\hat{\boldsymbol{p}}_i$ is the virtual momenta of the atom i. $\hat{\boldsymbol{q}} = (\hat{\boldsymbol{q}}_1, \hat{\boldsymbol{q}}_2, \hat{\boldsymbol{q}}_3, \ldots, \hat{\boldsymbol{q}}_N)$, where $\hat{\boldsymbol{q}}_i$ is the virtual coordinates of the ith atom, and N is the number of atoms. m_i is the mass of the ith atom. U is the potential energy. T is the target temperature. π and s are the conjugate pair describing a thermostat. Q is the artificial mass associated with s. P is the target pressure. P_V and V are the conjugate pair describing a barostat. W is the artificial mass associated with V. The value of the constant H_0 is chosen so that H is zero at the initial time ($t = 0$). The real momenta $\boldsymbol{p}_i$ and coordinates $\boldsymbol{q}_i$ are given by the relations $\boldsymbol{p}_i = \hat{\boldsymbol{p}}_i/V^{\frac{1}{3}}s$ and $\boldsymbol{q}_i = V^{\frac{1}{3}}\hat{\boldsymbol{q}}_i$, respectively.

The time evolution of a quantity $A(\boldsymbol{\Gamma}(t))$ in the phase space $\boldsymbol{\Gamma} = (\hat{\boldsymbol{q}}, \hat{\boldsymbol{p}}, s, \pi, V, P_V)$ from time t to time $t + \Delta t$ is described as

$$A[\boldsymbol{\Gamma}(t + \Delta t)] = \exp(D_H \Delta t) A[\boldsymbol{\Gamma}(t)]. \tag{A2}$$

Here $\exp(D_H \Delta t)$ is the time evolution operator, and the operator D_H is defined by

$$D_H \equiv \dot{\boldsymbol{\Gamma}} \cdot \frac{\partial}{\partial \boldsymbol{\Gamma}}. \tag{A3}$$

We follow Nosé's approach [42] to formulate an explicit symplectic integrator and decompose H into the following four terms:

$$H = H_1 + H_2 + H_3 + H_4, \tag{A4}$$

where

$$H_1 = s\left[\sum_{i=1}^{N}\frac{\hat{\boldsymbol{p}}_i^2}{2m_i V^{\frac{2}{3}}s^2} + 3Nk_{\mathrm{B}}T\ln(s) + PV - H_0\right], \quad \text{(A5)}$$

$$H_2 = \frac{sP_V^2}{2W}, \quad \text{(A6)}$$

$$H_3 = sU(V^{\frac{1}{3}}\hat{\boldsymbol{q}}), \quad \text{(A7)}$$

$$H_4 = \frac{s\pi^2}{2Q}. \quad \text{(A8)}$$

We then decompose D_H into four terms as follows:

$$D_H = D_{H_1} + D_{H_2} + D_{H_3} + D_{H_4}, \quad \text{(A9)}$$

where

$$\begin{aligned} D_{H_1} &= -\sum_{i=1}^{N}\left\{\frac{\partial H_1}{\partial\hat{\boldsymbol{q}}_i}\frac{\partial}{\partial\hat{\boldsymbol{p}}_i} - \frac{\partial H_1}{\partial\hat{\boldsymbol{p}}_i}\frac{\partial}{\partial\hat{\boldsymbol{q}}_i}\right\} - \frac{\partial H_1}{\partial s}\frac{\partial}{\partial\pi} \\ &\quad + \frac{\partial H_1}{\partial\pi}\frac{\partial}{\partial s} - \frac{\partial H_1}{\partial V}\frac{\partial}{\partial P_V} + \frac{\partial H_1}{\partial P_V}\frac{\partial}{\partial V} \\ &= \sum_{i=1}^{N}\frac{\hat{\boldsymbol{p}}_i}{m_i V^{\frac{2}{3}}s}\frac{\partial}{\partial\hat{\boldsymbol{q}}_i} \\ &\quad + \left\{\sum_{i=1}^{N}\frac{\hat{\boldsymbol{p}}_i^2}{2m_i V^{\frac{2}{3}}s^2} - 3Nk_{\mathrm{B}}T[1+\ln(s)] - PV + H_0\right\}\frac{\partial}{\partial\pi} \\ &\quad + s\left(\frac{2}{3V}\sum_{i=1}^{N}\frac{\hat{\boldsymbol{p}}_i^2}{2m_i V^{\frac{2}{3}}s^2} - P\right)\frac{\partial}{\partial P_V}, \end{aligned} \quad \text{(A10)}$$

$$D_{H_2} = -\frac{P_V^2}{2W}\frac{\partial}{\partial\pi} + s\frac{P_V}{W}\frac{\partial}{\partial V}, \quad \text{(A11)}$$

$$\begin{aligned} D_{H_3} &= \sum_{i=1}^{N} sV^{\frac{1}{3}}\boldsymbol{F}_i\frac{\partial}{\partial\,\hat{\boldsymbol{p}}_i} - U(V^{\frac{1}{3}}\hat{\boldsymbol{q}})\frac{\partial}{\partial\pi} \\ &\quad + s\left(P_{\mathrm{ins}} - \frac{Nk_{\mathrm{B}}T_{\mathrm{ins}}}{V}\right)\frac{\partial}{\partial P_V}, \end{aligned} \quad \text{(A12)}$$

$$D_{H_4} = -\frac{\pi^2}{2Q}\frac{\partial}{\partial\pi} + \frac{s\pi}{Q}\frac{\partial}{\partial s}. \quad \text{(A13)}$$

Here P_{ins} and T_{ins} are instantaneous pressure and temperature, respectively. Note that

$$P_{\mathrm{ins}} = \frac{Nk_{\mathrm{B}}T_{\mathrm{ins}}}{V} + \frac{1}{3V}\sum_{i=1}^{N}(V^{\frac{1}{3}}\hat{\boldsymbol{q}}_i)\cdot\boldsymbol{F}_i, \quad \text{(A14)}$$

$$T_{\mathrm{ins}} = \frac{2}{3Nk_{\mathrm{B}}}\sum_{i=1}^{N}\frac{\hat{\boldsymbol{p}}_i^2}{2m_i V^{\frac{2}{3}}s^2}, \quad \text{(A15)}$$

$$\frac{\partial}{\partial\hat{\boldsymbol{q}}_i}sU(V^{\frac{1}{3}}\hat{\boldsymbol{q}}) = sV^{\frac{1}{3}}\left[\frac{\partial U(\boldsymbol{q})}{\partial\boldsymbol{q}_i}\right]_{\boldsymbol{q}=V^{\frac{1}{3}}\hat{\boldsymbol{q}}} = -sV^{\frac{1}{3}}\boldsymbol{F}_i, \quad \text{(A16)}$$

$$\begin{aligned} \frac{\partial}{\partial V}sU(V^{\frac{1}{3}}\hat{\boldsymbol{q}}) &= s\sum_{i=1}^{N}\left(\frac{1}{3}V^{-\frac{2}{3}}\hat{\boldsymbol{q}}_i\right)\cdot\left[\frac{\partial U(\boldsymbol{q})}{\partial\boldsymbol{q}_i}\right]_{\boldsymbol{q}=V^{\frac{1}{3}}\hat{\boldsymbol{q}}} \\ &= -s\frac{1}{3V}\sum_{i=1}^{N}(V^{\frac{1}{3}}\hat{\boldsymbol{q}}_i)\cdot\boldsymbol{F}_i \\ &= -s\left(P_{\mathrm{ins}} - \frac{Nk_{\mathrm{B}}T_{\mathrm{ins}}}{V}\right). \end{aligned} \quad \text{(A17)}$$

We neglect the terms of order higher than two in Δt and obtain

$$\begin{aligned} &\exp(D_H\Delta t) \\ &\approx \exp\left(\frac{D_{H_4}\Delta t}{2}\right)\exp\left(\frac{D_{H_3}\Delta t}{2}\right)\exp\left(\frac{D_{H_2}\Delta t}{2}\right) \\ &\quad\times\exp\left(D_{H_1}\Delta t\right)\exp\left(\frac{D_{H_2}\Delta t}{2}\right)\exp\left(\frac{D_{H_3}\Delta t}{2}\right) \\ &\quad\times\exp\left(\frac{D_{H_4}\Delta t}{2}\right). \end{aligned} \quad \text{(A18)}$$

Finally, the time evolution of the system is described as follows:

(1) Operation of $\exp\left(\frac{D_{H_4}\Delta t}{2}\right)$:

$$s^{(n+\frac{1}{2})} = s^{(n)}\left(1 + \frac{\pi^{(n)}}{2Q}\frac{\Delta t}{2}\right)^2,$$

$$\pi^{(*1)} = \frac{\pi^{(n)}}{1 + \frac{\pi^{(n)}}{2Q}\frac{\Delta t}{2}}.$$

(2) Operation of $\exp\left(\frac{D_{H_3}\Delta t}{2}\right)$:

$$\hat{\boldsymbol{p}}_i^{(n+\frac{1}{2})} = \hat{\boldsymbol{p}}_i^{(n)} + s^{(n+\frac{1}{2})}\{V^{(n)}\}^{\frac{1}{3}}\boldsymbol{F}_i^{(n)}\frac{\Delta t}{2},$$

$$\pi^{(*2)} = \pi^{(*1)} - U^{(n)}\frac{\Delta t}{2},$$

$$P_V^{(*1)} = P_V^{(n)} + s^{(n+\frac{1}{2})}\left(P_{\mathrm{ins}}^{(n)} - \frac{Nk_{\mathrm{B}}T_{\mathrm{ins}}^{(n)}}{V^{(n)}}\right)\frac{\Delta t}{2}.$$

(3) Operation of $\exp\left(\frac{D_{H_2}\Delta t}{2}\right)$:

$$\pi^{(*3)} = \pi^{(*2)} - \frac{\left\{P_V^{(*1)}\right\}^2}{2W}\frac{\Delta t}{2},$$

$$V^{(n+\frac{1}{2})} = V^{(n)} + s^{(n+\frac{1}{2})}\frac{P_V^{(*1)}}{W}\frac{\Delta t}{2}.$$

(4) Operation of $\exp\left(D_{H_1}\Delta t\right)$:

$$\hat{\boldsymbol{q}}_i^{(n+1)} = \hat{\boldsymbol{q}}_i^{(n)} + \frac{\hat{\boldsymbol{p}}_i^{(n+\frac{1}{2})}}{m_i\left\{V^{(n+\frac{1}{2})}\right\}^{\frac{2}{3}}s^{(n+\frac{1}{2})}}\Delta t,$$

$$\pi^{(*4)} = \pi^{(*3)} + \left[\sum_{i=1}^{N}\frac{1}{2m_i}\left(\frac{\hat{\boldsymbol{p}}_i^{(n+\frac{1}{2})}}{\{V^{(n+\frac{1}{2})}\}^{\frac{1}{3}}s^{(n+\frac{1}{2})}}\right)^2 - 3Nk_{\mathrm{B}}T\left(1+\ln s^{(n+\frac{1}{2})}\right) - PV^{(n+\frac{1}{2})} + H_0\right]\Delta t,$$

$$P_V^{(*2)} = P_V^{(*1)} + s^{(n+\frac{1}{2})} \times \left[\frac{2}{3V^{(n+\frac{1}{2})}} \sum_{i=1}^{N} \frac{1}{2m_i} \left(\frac{\hat{\boldsymbol{p}}_i^{(n+\frac{1}{2})}}{\{V^{(n+\frac{1}{2})}\}^{\frac{1}{3}} s^{(n+\frac{1}{2})}} \right)^2 - P \right] \Delta t.$$

(5) Operation of $\exp(\frac{D_{H_2}\Delta t}{2})$:

$$\pi^{(*5)} = \pi^{(*4)} - \frac{\{P_V^{(*2)}\}^2}{2W} \frac{\Delta t}{2},$$

$$V^{(n+1)} = V^{(n+\frac{1}{2})} + s^{(n+\frac{1}{2})} \frac{P_V^{(*2)}}{W} \frac{\Delta t}{2}.$$

(6) Operation of $\exp(\frac{D_{H_3}\Delta t}{2})$:

$$\hat{\boldsymbol{p}}_i^{(n+1)} = \hat{\boldsymbol{p}}_i^{(n+\frac{1}{2})} + s^{(n+\frac{1}{2})} \{V^{(n+1)}\}^{\frac{1}{3}} \boldsymbol{F}_i^{(n+1)} \frac{\Delta t}{2},$$

$$\pi^{(*6)} = \pi^{(*5)} - U^{(n+1)} \frac{\Delta t}{2},$$

$$P_V^{(n+1)} = P_V^{(*2)} + s^{(n+\frac{1}{2})} \left(P_{\text{ins}}^{(n+1)} - \frac{N k_{\text{B}} T_{\text{ins}}^{(n+1)}}{V^{(n+1)}} \right) \frac{\Delta t}{2}.$$

(7) Operation of $\exp(\frac{D_{H_4}\Delta t}{2})$:

$$s^{(n+1)} = s^{(n+\frac{1}{2})} \left(1 + \frac{\pi^{(*6)}}{2Q} \frac{\Delta t}{2} \right)^2,$$

$$\pi^{(n+1)} = \frac{\pi^{(*6)}}{1 + \frac{\pi^{(*6)}}{2Q} \frac{\Delta t}{2}}.$$

Here the superscript (n) in $s^{(n)}$, for example, represents the quantity s at the nth time step. $s^{(n+\frac{1}{2})}$, $\hat{\boldsymbol{p}}_i^{(n+\frac{1}{2})}$, $\pi^{(*1)}, \ldots, \pi^{(*6)}$, $V^{(n+\frac{1}{2})}$, $P_V^{(*1)}$, and $P_V^{(*2)}$ are intermediate variables.

[1] J. D. Bernal, Nature (London) **185**, 68 (1960).
[2] D. R. Nelson and F. Spaepen, Solid State Phys. **42**, 1 (1989).
[3] A. V. Anikeenko and N. N. Medvedev, Phys. Rev. Lett. **98**, 235504 (2007).
[4] D. Turnbull and R. E. Cech, J. Appl. Phys. **21**, 804 (1950).
[5] F. C. Frank, Proc. R. Soc. Lond. A **215**, 43 (1952).
[6] P. J. Steinhardt, D. R. Nelson, and M. Ronchetti, Phys. Rev. B **28**, 784 (1983).
[7] F. Yonezawa, Solid State Phys. **45**, 179 (1991).
[8] Y. Cheng and E. Ma, Prog. Mater. Sci. **56**, 379 (2011).
[9] S. Mossa and G. Tarjus, J. Chem. Phys. **119**, 8069 (2003).
[10] T. Schenk, D. Holland-Moritz, V. Simonet, R. Bellissent, and D. M. Herlach, Phys. Rev. Lett. **89**, 075507 (2002).
[11] A. Di Cicco, A. Trapananti, S. Faggioni, and A. Filipponi, Phys. Rev. Lett. **91**, 135505 (2003).
[12] K. Nishio, T. Miyazaki, and H. Nakamura, Phys. Rev. Lett. **111**, 155502 (2013).
[13] G. W. Lee, A. K. Gangopadhyay, K. F. Kelton, R. W. Hyers, T. J. Rathz, J. R. Rogers, and D. S. Robinson, Phys. Rev. Lett. **93**, 037802 (2004).
[14] A. Di Cicco, F. Iesari, S. De Panfilis, M. Celino, S. Giusepponi, and A. Filipponi, Phys. Rev. B **89**, 060102 (2014).
[15] F. Iesari and A. D. Cicco, J. Phys.: Conf. Ser. **712**, 012038 (2016).
[16] N. Jakse and A. Pasturel, Phys. Rev. Lett. **91**, 195501 (2003).
[17] N. Jakse, O. Le Bacq, and A. Pasturel, Phys. Rev. B **70**, 174203 (2004).
[18] A. Hirata, L. J. Kang, T. Fujita, B. Klumov, K. Matsue, M. Kotani, A. R. Yavari, and M. W. Chen, Science **341**, 376 (2013).
[19] F. H. Stillinger and R. A. LaViolette, Phys. Rev. B **34**, 5136 (1986).
[20] N. N. Medvedev, V. P. Voloshin, and Y. I. Naberukhin, J. Struct. Chem. **27**, 581 (1987).
[21] R. A. LaViolette, Phys. Rev. B **41**, 8526 (1990).
[22] A. Malins, S. R. Williams, J. Eggers, and C. P. Royall, J. Chem. Phys. **139**, 234506 (2013).
[23] J. D. Bernal, Nature (London) **183**, 141 (1959).
[24] M. A. Klatt and S. Torquato, Phys. Rev. E **90**, 052120 (2014).
[25] J. L. Finney, Philos. Mag. **93**, 3940 (2013).
[26] T. C. Hales and S. McLaughlin, J. Amer. Math. Soc. **23**, 299 (2010).
[27] K. Nishio and T. Miyazaki, Sci. Rep. **6**, 23455 (2016).
[28] K. Nishio and T. Miyazaki, Sci. Rep. **7**, 40269 (2017).
[29] K. Nishio and T. Miyazaki, Polyhedron and polychoron codes for describing atomic arrangements, in *Nanoinformatics*, edited by I. Tanaka (Springer, Singapore, 2018), pp. 97–130.
[30] S.-P. Pan, S.-D. Feng, J.-W. Qiao, W.-M. Wang, and J.-Y. Qin, Sci. Rep. **5**, 16956 (2015).
[31] M. Tanaka, J. Phys. Soc. Jpn. **55**, 3428 (1986).
[32] E. A. Lazar, J. K. Mason, R. D. MacPherson, and D. J. Srolovitz, Phys. Rev. Lett. **109**, 095505 (2012).
[33] G. Galilei, *Il Saggiatore* (Passerino Editore, Rome, 2017).
[34] R. Kurita and E. R. Weeks, Phys. Rev. E **82**, 011403 (2010).
[35] K. Nishio and M. Mikami, J. Chem. Phys. **130**, 154302 (2009).
[36] L. Weinberg, IEEE Trans. Circuit Theory **13**, 142 (1966).
[37] J.-P. Hansen and I. R. McDonald, *Theory of Simple Liquids*, 2nd ed. (Academic Press, 1990).
[38] H. Heinz, B. L. Farmer, and R. R. Naik, J. Phys. Chem. C **112**, 17281 (2008).
[39] E. A. Mastny and J. J. de Pablo, J. Chem. Phys. **127**, 104504 (2007).
[40] S. Nosé, J. Chem. Phys. **81**, 511 (1984).
[41] S. D. Bond, B. J. Leimkuhler, and B. B. Laird, J. Comput. Phys. **151**, 114 (1999).
[42] S. Nosé, J. Phys. Soc. Jpn. **70**, 75 (2001).
[43] H. C. Andersen, J. Chem. Phys. **72**, 2384 (1980).
[44] S. Nosé, Mol. Phys. **52**, 245 (1984).
[45] M. N. Bannerman, R. Sargant, and L. Lue, J. Comput. Chem. **32**, 3329 (2011).
[46] G. van Anders, D. Klosta, N. K. Ahmed, M. Engel, and S. C. Glotzer, Proc. Natl. Acad. Sci. USA **111**, E4812 (2014).
[47] M. Leocmach and H. Tanaka, Nat. Commun. **3**, 974 (2012).